Journal of Materials Chemistry C

ROYAL SOCIETY OF CHEMISTRY

PAPER

View Article Online
View Journal | View Issue

Cite this: J. Mater. Chem. C, 2025, 13, 5545

A graphene-based tunable polarization insensitive terahertz metasurface absorber for multi-band high-efficiency applications

Taha Sheheryar,[a] Ye Tian,[b] Bo Lv,*[a] Xiuqin Chu*[c] and Jinhui Shi*[a]

Received 2nd January 2025,
Accepted 27th January 2025

DOI: 10.1039/d4tc05520a

rsc.li/materials-c

In this paper, we designed a novel tunable terahertz (THz) absorber that has unique properties of graphene integrated within a dual-layer metasurface structure. The proposed absorber demonstrates excellent performance by achieving eight distinct absorption peaks from 3.9 THz to 9.73 THz with an average absorption efficiency of 99.3%. This is achieved through the tunable surface conductivity of graphene which enables dynamic modulation of resonant frequencies *via* chemical potential adjustment. The design includes a gold base layer for total reflection, gallium arsenide (GaAs) dielectric spacers for optimum impedance matching and graphene patches to introduce multi-band absorption modes. Simulation results show the absorber's tunability, polarization insensitivity and angular stability which makes it highly adaptable for applications in medical diagnostics, material characterization, security screening and terahertz sensing. The proposed absorber's innovative architecture and simple design offers a versatile solution for the evolving demands of modern terahertz technologies.

1. Introduction

The terahertz region of the electromagnetic spectrum spans from nearly 100 GHz to 10 THz and inhabits a unique position between the microwave and infrared regions.[1] This frequency range offers a distinct set of electromagnetic properties that are not found in lower or higher frequency bands. Terahertz radiation has the unique ability to interact with matter in ways that are highly advantageous for a wide range of applications. These include high resolution imaging,[2] material characterization,[3] spectroscopy[4] and communication technologies.[5] The terahertz waves can penetrate nonconductive materials such as clothing, paper and plastic but are blocked by metals and water which makes them ideal for nondestructive testing and security screening.[6,7] They can also provide highly detailed information about the molecular and structural composition of materials without causing any damage which makes terahertz technology increasingly vital in fields of thermal emitting, environmental monitoring and chemical analysis.[8–10]

Traditional metamaterial absorbers (MMAs) naturally rely on metal–dielectric–metal configuration which are usually limited by their fixed operational frequency bands. Once these absorbers are fabricated their performance at specific frequencies cannot be adjusted. This limits their usefulness and applicability in active environments. The unique ability to selectively manipulate and absorb multiple distinct frequencies provides significant opportunities for advancing signal processing capabilities that include enhancement in imaging resolution and strengthening security protocols across a range of applications. The integration of graphene into these designs provide a transformative solution to the said restraint. When coupled with micro or nanostructures, graphene can engage in surface plasmon resonance especially in the terahertz and infrared regions.[11] One of the most significant advantages of graphene-based metamaterial absorbers is the ability to dynamically adjust the absorber's operational frequency band. This is achieved through the external modulation of graphene's chemical potential *via* an applied bias voltage which effectively alters its surface conductivity distribution.[12,13] Tuning the chemical potential results in a change in the resonant frequency of the absorber which can be precisely controlled and this offers unparalleled flexibility in adapting to different terahertz frequencies.[14–16] This tunability is an essential feature for terahertz applications where real-time adjustment is vital for various sensing and communication applications.[17,18]

In addition to graphene, other materials are frequently used in combination with graphene to enhance the performance of

[a] Key Laboratory of In-Fiber Integrated Optics of Ministry of Education, College of Physics and Optoelectronic Engineering, Harbin Engineering University, Harbin 150001, Heilongjiang Province, China. E-mail: lb19840313@126.com, shijinhui@hrbeu.edu.cn
[b] College of Automation, Nanjing University of Science and Technology, Nanjing 210000, Jiangsu Province, China
[c] Key Laboratory of High-Speed Circuit Design and EMC Ministry of Education, Xidian University, Xi'an, 710071, China. E-mail: xqchu@mail.xidian.edu.cn

terahertz metamaterial absorbers. Silicon (Si) is often utilized as a dielectric spacer material due to its well-established compatibility with nanofabrication processes and its excellent dielectric properties.[19,20] Gold (Au) is known for its outstanding electrical conduction and ease of processing and is often used as the metal layer in metamaterial designs mostly as the ground plane or for forming resonant structures. Combining graphene with silicon and gold effectively creates high-efficiency terahertz absorbers with strong multi-band performance.[21,22] Researchers have also discovered the use of materials such as aluminum (Al), silver (Ag) and copper (Cu) in their designs where each element has specific advantages depending on the desired outcome of the absorber. For example, aluminum is frequently used due to its low cost and ease of fabrication while silver is valued for its high conductivity.[23,24] Furthermore, materials like GaAs and silicon dioxide (silica) have been commonly used as substrates to provide excellent dielectric properties which confirms the stable and effective performance of the absorber. GaAs, with its high refractive index and strong compatibility with graphene, enhances the coupling between the graphene layers and the incident terahertz radiation and improves the absorption efficiency.[25,26] Silica on the other hand is often utilized for its transparency to terahertz waves and favorable dielectric constant which aids in upholding the performance of the absorber while also ensuring structural stability.[27,28] Metamaterial absorbers composed of graphene and these matching materials have demonstrated the ability to achieve high absorption efficiencies across a broad range of terahertz frequencies.[29] These designs are vital for widespread applications in terahertz technologies where operating in a broad frequency range is often required. Moreover, these absorbers also exhibit polarization insensitivity which is a highly required feature in many practical applications as it allows for reliable performance regardless of the angle or polarization of the incoming terahertz radiation.[30,31] Recently complex, multi-layer structures stacked on one another to create terahertz absorbers were developed and used. These hybrid materials provide a wide range of tunable electronic and optical properties that can be used to achieve greater flexibility and performance in terahertz absorption.[32] By merging materials with matching property elements such as the high electrical conductivity of graphene with the strong dielectric properties of silicon, researchers are able to create absorbers with extraordinary performance that include high efficiency, tunability and broad bandwidths.[33]

In this paper, we present a novel design for a tunable terahertz absorber that structures a two-layer design that joins the tunable properties of graphene to achieve broadband, multi-peak absorption across the terahertz spectrum. The design consists of a gold base layer, a GaAs dielectric spacer and a graphene layer placed at the center of the unit cell from bottom to top. This is added by a second GaAs spacer and four graphene patches at the corners of the unit cell which further improve the interaction between terahertz radiation and the absorber. The ability to precisely tune the absorption peaks by controlling the chemical potential of graphene offers high flexibility and efficiency in controlling the absorption performance at specific terahertz frequencies. The key feature of this design is its ability to generate eight sharp absorption peaks spanning from 3.9 THz to 9.73 THz with seven peaks exceeding 99.9% absorption efficiency and one peak at 97.4% absorption and therefore resulting in a total absorption average of 99.3%. These absorption peaks occur at frequencies of 3.9 THz, 4.67 THz, 5.5 THz, 6.35 THz, 7.2 THz, 8.05 THz, 8.9 THz and 9.73 THz. The precise tuning of these peaks is accomplished by regulating the Fermi level (E_f) of the graphene which permits selective absorption at various frequencies. This high level of accuracy makes the design suitable for applications requiring fine control over frequency selection.

Simulation results reveal that the key parameters such as the Fermi level of graphene, relaxation time, graphene temperature and arrangement of the graphene patches significantly affect the absorption performance. Detailed parametric analyses show that the Fermi level directly affects the placement and sharpness of the absorption peaks that allow fine-tuning of the design. The relaxation time also influences the rate at which the graphene's surface conductivity adjusts to the Terahertz field which enhances the efficiency of the absorber. The electric field distribution within the structure demonstrates the resonant modes shaped by the graphene patches which confirms the effective interaction between the terahertz waves and the absorber's material. The high efficiency multi-peak absorption design we proposed delivers a multipurpose solution for broadly applicable terahertz technologies that include medical diagnostics, material analysis, security screening and non-destructive testing.[34,35] The key innovations in our design include its simple and scalable configuration which reduces fabrication complexity while maintaining high efficiency. The design achieves eight precisely almost equidistant absorption peaks and offers tunability across a wider bandwidth than previously reported absorbers. This unique arrangement is particularly suited for applications requiring selective frequency absorption and fine-tuned resonance such as early cancer detection, material characterization and public safety screening.

2. Discussion and analysis

2.1. Unit cell design

The unit cell of the proposed terahertz absorber is designed in a way to achieve multi-peak tunable absorption across the terahertz spectrum of 3.9 THz to 9.7 THz. The design comprises a multi-layer structure that makes the best use of the interaction between terahertz waves and the absorber's material that exploits the unique properties of graphene that enable tunable absorption. The structure starts with a lossy gold base layer with the conductivity $\sigma = 4.561 \times 10^7$ S m^{-1} and is placed at the bottom of the unit cell. Gold's high conductivity ensures that Terahertz waves are reflected back into the structure, prevents transmission and promotes multiple internal reflections. This reflection maximizes the interaction of the terahertz waves with the absorber which enhances the absorption efficiency. The gold base layer plays a key role in ensuring that the terahertz radiation is confined within the structure for optimal

absorption. Above the gold base is a GaAs dielectric spacer. This GaAs spacer is 45 μm thick and serves two primary purposes. Firstly, it helps to optimize the interaction between the incident terahertz waves and the graphene layer. Secondly, it provides the necessary dielectric environment required for resonance. GaAs with its high dielectric constant ε_r = 12.94 and tangent loss of tan δ = 0.006 allows efficient impedance matching and reduces energy losses during the propagation of terahertz waves through the structure.

The central graphene layer which is placed above the GaAs spacer is the active material responsible for tuning the absorption. The graphene layer with a thickness of 1 nm has the unique ability to modulate its surface conductivity and Fermi level through an external voltage. This allows the tunable absorption that defines the performance of the absorber. With a relaxation time of τ = 0.1 ps, a chemical potential of 1.5 eV and a temperature of 300 K, graphene can be adjusted to selectively absorb terahertz radiation at specific frequencies which provides flexibility and precision in applications requiring dynamic frequency tuning.

Sitting on top of the central graphene layer is another GaAs dielectric spacer. This second GaAs spacer is 5 μm thick which isolates the graphene patches positioned at the corners of the unit cell from the central graphene layer. All graphene patches are 15 μm × 15 μm wide and introduce additional resonant modes that allow multi-band absorption at different terahertz frequencies. The patches further enhance the sharpness and definition of the absorption peaks which improves the overall performance of the absorber. The strategic positioning of these patches at the top corners ensures that they interact with the incident terahertz waves independently and promote multi-frequency absorption.

In Fig. 1(a) the perspective view of the unit cell is presented which provides an overview of the entire structure from the gold base layer to the graphene patches. Fig. 1(b) illustrates the layer-by-layer breakdown of the structure showing the thickness and positioning of each layer including the gold base, GaAs spacers, central graphene layer and the top graphene patches. The preparation process of the dual-layer graphene metasurface absorber is detailed in Fig. 2. Initially, the dielectric structure is deposited onto the metallic base (Au) using physical vapor deposition (PVD) to ensure a stable foundation.

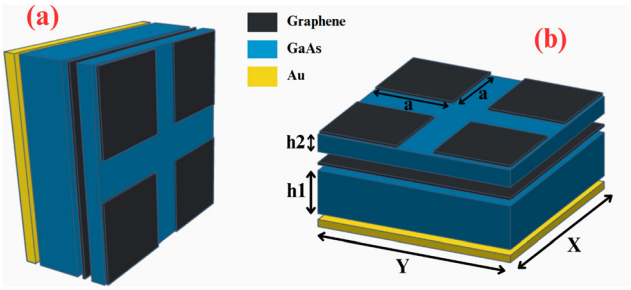

Fig. 1 Schematic of the metasurface absorber design. (a) Perspective view of the unit cell. (b) Layered view showing the dimensions of the unit cell with $X = Y$ = 36 μm, a = 15 μm, $h1$ = 45 μm and $h2$ = 5 μm, representing the gold base GaAs spacer and graphene layers.

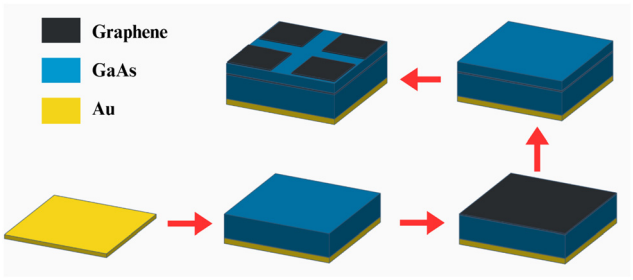

Fig. 2 Fabrication process of the dual-layer graphene metasurface absorber.

For the graphene sheet, graphene is synthesized *via* chemical vapor deposition (CVD) on a copper catalyst. The isolation layer is then transferred onto the GaAs dielectric spacer using a wet transfer method which ensures minimal defects and maintains the graphene's electronic properties. To realize the precise dual-layer patterned graphene configuration, electron beam lithography (EBL) is employed which is followed by oxygen plasma etching (OPE) to remove any undesired portions and achieve the desired geometric pattern.[36] Finally, the photoresist is stripped, resulting in the dual-layer graphene metasurface absorber design ready for use in terahertz applications.

To analyze and optimize the proposed metasurface absorber, simulations were performed using CST Studio Suite 2019 which is a commercially available electromagnetic simulation software. Periodic boundary conditions were applied along the x and y directions to ensure the periodicity of the metasurface design while an open boundary condition was set along the z direction to permit wave propagation. A plane wave was incident from the negative z direction with the electric field polarized along the y-axis to certify precise simulation of electromagnetic interactions. For high precision and accuracy, a fine-tuned tetrahedral mesh was employed with 178 778 elements. Careful adjustments were made to accurately model the unique properties of the graphene layer and the geometric dimensions of the unit cell were meticulously optimized to achieve multi-peak absorption across the terahertz range. The design stands out by combining simplicity with scalability. In other words, it offers a structure that is easier to fabricate compared to the intricate patterns used in many existing designs while achieving an unprecedented bandwidth of 3.9–9.73 THz with eight distinct absorption peaks.

2.2. Theory and method

The absorption behavior of the metamaterial is mainly determined by the resonant interaction between the incident terahertz radiation and the resonant modes of the metasurface absorber's structure. Resonance occurs when the frequency of the incident terahertz wave aligns with the natural frequency of the resonant modes within the metamaterial which leads to effective energy transfer from the incident wave to the absorber and converting it into other forms of energy like heat, *etc.* The key instrument behind the resonance is the tuning of the graphene's surface conductivity which is controlled by applying a bias voltage to the material. The surface conductivity of

graphene as a two-dimensional material is highly tunable which allows for the modulation of its resonance frequency in the terahertz range. This tunability is essential for creating a flexible, multi-peak absorption spectrum. The surface conductivity $\sigma(\omega)$ of graphene can be expressed in terms of the Kubo formula for frequency-dependent conductivity:[37]

$$\sigma(\omega) = \sigma_{\text{inter}}(\omega) + \sigma_{\text{intra}}(\omega) \quad (1)$$

where $\sigma_{\text{inter}}(\omega)$ and $\sigma_{\text{intra}}(\omega)$ are the inter-band and intra-band conductivities of the graphene and can be expressed using the classical Kubo formula.[38]

$$\sigma_{\text{inter}}(\omega) = \frac{ie^2}{4n\hbar^2}\ln\left[\frac{2E_f - \hbar(\omega + i\tau^{-1})}{2E_f + \hbar(\omega + i\tau^{-1})}\right] \quad (2)$$

$$\sigma_{\text{intra}}(\omega) = \frac{ie^2 K_B T}{n\hbar^2(\omega + i\tau^{-1})}\left\{\frac{E_f}{K_B T} + 2\ln\left[\exp\left(-\frac{E_f}{K_B T}\right) + 1\right]\right\} \quad (3)$$

where 'e' is the electron charge (1.6×10^{-19} C), $\hbar$ is the reduced Planck constant, E_f is the Fermi energy of graphene, τ is the angular frequency of the incident terahertz radiation, τ is the relaxation time graphene, K_B denotes the Boltzmann constant and T represents time in Kelvin. At terahertz frequencies, the inter-band transitions become negligible due to the large Fermi energy $E_f \gg K_B T$, simplifying the expression for conductivity to the Drude model:[39]

$$\sigma(\omega) = \frac{ie^2 E_f}{n\hbar^2(\omega + i\tau^{-1})} \quad (4)$$

This conductivity formula governs the interaction of graphene with the incident terahertz waves and defines the resonance condition of the absorber. The multi-peak absorption behavior observed in the design results is formed due to the excitation of multiple resonant modes within the unit cell of the metamaterial. Each resonant mode corresponds to a distinct absorption peak in the terahertz spectrum. The precise frequency of each peak is influenced by the size and placement of the graphene patches as well as the dielectric constant of the spacer material. By tuning the chemical potential 'E_f' of graphene the resonant frequencies can be adjusted which allows dynamic control over the absorption peaks. The sharpness of these peaks is influenced by the relaxation time 'τ'. With shorter relaxation times, reducing the coupling between the incident waves and the graphene layer leads to sharper and more distinct absorption peaks.

Moreover, the absorption efficiency $A(\omega)$ of the proposed terahertz metasurface absorber can be calculated using its S-parameters which describe the transmission and reflection characteristics of the absorber at a given frequency. The absorption efficiency is expressed as:[40]

$$A(\omega) = 1 - T(\omega) - R(\omega) = 1 - {S_{21}}^2 - {S_{11}}^2 \quad (5)$$

where $T(\omega) = {S_{21}}^2$ is the transmission coefficient which represents the portion of the incident wave that passes through the absorber and $R(\omega) = {S_{11}}^2$ is the reflection coefficient which indicates the fraction of the incident wave that is reflected back. Since the design incorporates a gold layer as the base therefore it acts as a perfect reflector for the incident terahertz waves. The high conductivity of gold ensures that the majority of the incident terahertz radiation is reflected back into the structure which minimizes transmission and prevents energy loss through the backside. Due to the continuous gold base layer, the transmissivity is nearly zero and effectively eliminates transmission. As a result, the absorption can be simplified as:

$$A(\omega) = 1 - R(\omega) = 1 - {S_{11}}^2 \quad (6)$$

here the absorption is solely determined by the reflection coefficient ${S_{11}}^2$ which reflects the portion of the incident wave that is reflected by the metasurface. In addition to gold, the dielectric materials (GaAs) further enhance the reflection by optimizing the impedance matching between the incident wave and the metasurface structure. These materials help control the phase of the reflected wave and minimize any potential energy losses that contribute to the sharpness and strength of the absorption peaks. Thus, the combined effect of the gold reflector and the dielectric spacers results in nearly perfect reflection and consequently high absorption efficiency. As shown in Fig. 3(a), the metasurface absorber exhibits eight distinct absorption peaks at 3.9 THz, 4.67 THz, 5.5 THz, 6.35 THz, 7.2 THz, 8.05 THz, 8.9 THz and 9.73 THz with absorption efficiencies of 99.08%, 99.94%, 99.37%, 99.57%, 99.94%, 99.91%, 99.30%, and 97.44%, respectively. These peaks correspond to highly efficient absorption with seven of the eight peaks exceeding 99.9% absorption efficiency. The average absorption across all these peaks is

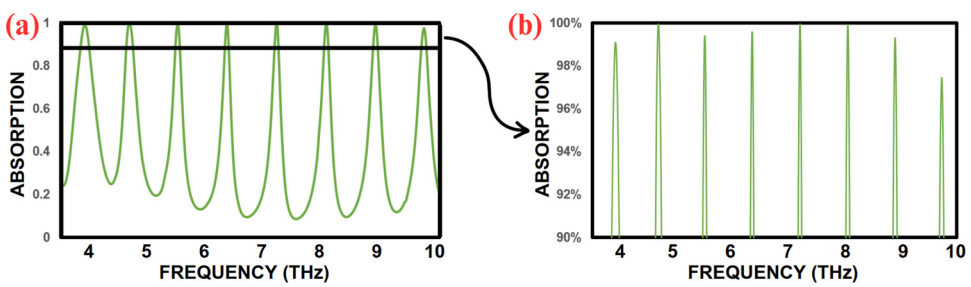

Fig. 3 Absorption performance of the proposed metasurface absorber. (a) The overall absorption spectrum showing eight distinct absorption peaks at 3.9 THz, 4.67 THz, 5.5 THz, 6.35 THz, 7.2 THz, 8.05 THz, 8.9 THz and 9.73 THz with high efficiencies. (b) A zoomed-in view of the absorption peaks above 90%, highlighting the sharp and distinct nature of each peak.

calculated to be approximately 99.3% which reflects the overall high performance of the proposed metasurface. The distinct spacing between these peaks which range from 3.9 THz to 9.73 THz, provides a broad bandwidth that is highly beneficial for applications requiring multiple frequency bands. This unique separation allows for selective targeting of specific terahertz frequencies which makes the metasurface absorber suitable for various applications such as terahertz sensing, material characterization and imaging. Fig. 3(b) provides a more detailed view of these absorption peaks above 90% and emphasizes the sharp and well-defined nature of each peak.

2.3. Parametric analysis

The parametric analysis delves into the effects of critical design and material parameters on the performance of the proposed metasurface absorber which focuses specifically on its absorption peaks and overall tunability. By systematically varying these parameters, especially the chemical potential of graphene (eV), the size of the top graphene patch (a), the operating temperature of graphene (T) and the relaxation time (τ), we can discern their significant influence on the resonance frequencies and absorption efficiency of the device. Fig. 4 illustrates the impact on the absorption peaks of the proposed metasurface absorber upon varying the chemical potential (eV) of both the graphene layers using an externally applied bias voltage. This analysis underscores the highly tunable characteristics of the absorber, as the resonance frequencies shift progressively with changes in the chemical potential. Fig. 4(a) showcases the full absorption spectrum from 3.5 THz to 10 THz for three distinct chemical potential values *i.e.* 1 eV, 1.5 eV and 2 eV. The peaks for 1 eV are consistently positioned behind those for 1.5 eV which in turn trail those for 2 eV. This clear forward shift in resonance frequencies with increasing eV illustrates the dynamic adaptability of the graphene-based metasurface absorber. The demonstrated tunability achieved through precise modulation of the chemical potential is a defining feature of the absorber. This capability not only validates the absorber's versatility but also highlights its potential for applications requiring fine frequency adjustments, even in the lower THz ranges. Such a design ensures that the absorber can cater to a wide array of practical and advanced terahertz sensing and imaging technologies.

Fig. 4(b)–(d) provide a detailed view of selected absorption peaks and focus on regions where absorption efficiency exceeds 80%. Fig. 4(b) zooms in on the absorption peak near 6.347 THz. At 1.5 eV, the maximum absorption occurs at 6.347 THz, whereas for 1 eV and 2 eV the peaks shift to 6.321 THz and 6.372 THz respectively. Similarly, Fig. 4(c) highlights the absorption peak near 7.2 THz. The peak for 1.5 eV is located at 7.205 THz while the peaks for 1 eV and 2 eV occur at 7.172 THz and 7.231 THz respectively further demonstrating the forward movement of the peaks with increasing eV. Fig. 4(d) focuses on the peak near 8.056 THz where the maximum absorption for 1.5 eV is at 8.056 THz for 1 eV at 8.0175 THz and for 2 eV at 8.089 THz. These observations consistently show that higher chemical potential values result in absorption peaks shifting to higher frequencies. This high degree of tunability demonstrates the potential of the proposed metasurface absorber for applications requiring adaptive resonance frequencies. For instance, in Fig. 4(b), the tunability enables fine control within a narrow band near 6.35 THz while in Fig. 4(c) and (d) the absorber achieves similar control in the 7.2 THz and 8.05 THz regions, respectively.

Fig. 5 illustrates the effect of relaxation time (τ) and operating temperature on the absorption spectrum of the proposed metasurface absorber. In Fig. 5(a), the absorption performance

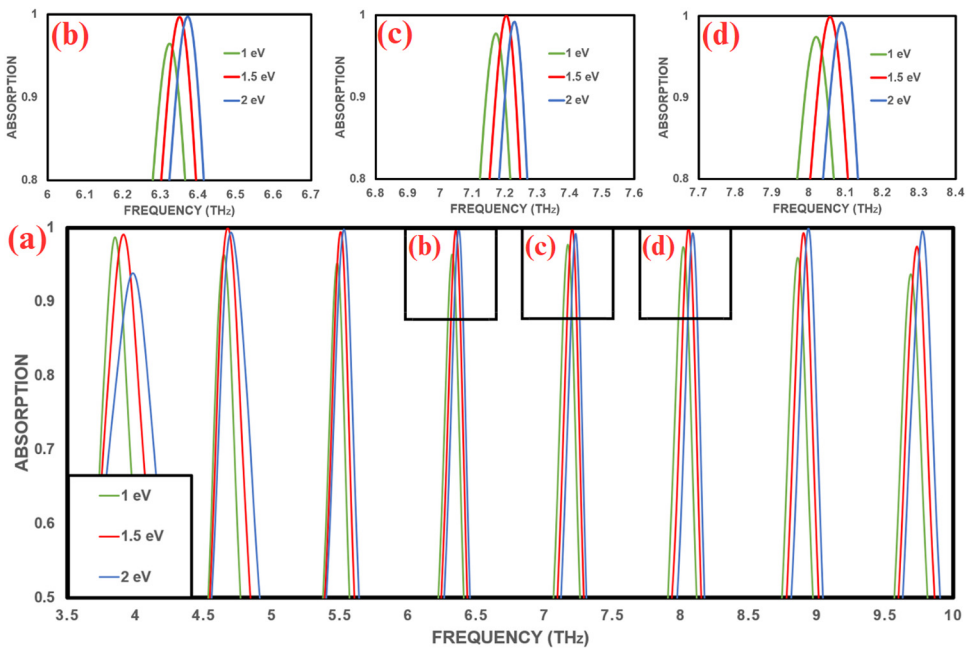

Fig. 4 Absorption spectrum of graphene at chemical potentials of 1, 1.5, and 2 eV. (a) Complete spectrum (3.5–10 THz) showing tunable peak shifts. (b)–(d) Close-ups of peaks near 6.35 THz, 7.2 THz and 8.05 THz.

is analyzed for three relaxation time values *i.e.*, 0.1 ps, 0.3 ps, and 0.5 ps. It is observed that as τ increases, there is a slight reduction in absorption efficiency especially at lower frequencies. Although the absorption remains above 90% even at τ = 0.5 ps, a minor redshift in the resonance peaks is observed with increasing τ which is attributed to reduced coupling efficiency between the terahertz waves and the graphene surface. The highest absorption and sharpest peaks occur at τ = 0.1 ps which makes it the optimal choice for this design to achieve superior performance in the desired frequency range. Fig. 5(b) examines the absorption spectrum at different operating temperatures *i.e.*, 275 K, 300 K and 325 K. The results reveal that variations in temperature have a negligible impact on the absorption characteristics with the resonance frequencies and peak efficiencies remaining nearly identical across all temperatures. This temperature insensitivity underscores the robustness of the metasurface absorber which ensures stable performance under varying environmental conditions. Such stability is particularly advantageous for practical applications that require consistent absorption efficiency in dynamic thermal environments.

The size of the top graphene patch (a) plays a pivotal role in defining the resonant behavior and absorption efficiency of the metasurface absorber. As shown in Fig. 6, the absorption spectrum is highly dependent on '*a*' with the highest absorption achieved for a = 15 μm. The results demonstrate that as '*a*' decreases particularly below 7 μm, there is a noticeable reduction in absorption efficiency most significantly at lower frequencies. This occurs because the patch size directly influences the inductive and capacitive properties of the resonant structure which in turn determine the resonance frequency and coupling strength between the incident terahertz waves and the metasurface. Smaller patch sizes reduce the effective interaction area for the incident radiation hence weakening the resonance modes and leading to diminished absorption. Conversely, larger patch sizes provide stronger electromagnetic coupling and better confinement of the THz waves within the structure which results in sharper and more efficient absorption peaks.

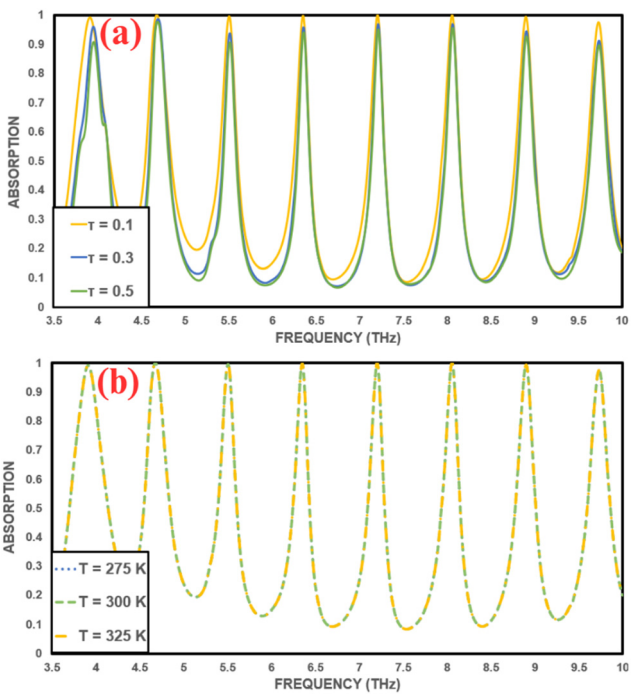

Fig. 5 (a) Absorption spectrum at relaxation times τ = 0.1 ps, 0.3 ps, and 0.5 ps showing slight absorption reduction and redshift with increasing τ. (b) Spectrum at T = 275 K, 300 K and 325 K showing temperature insensitivity.

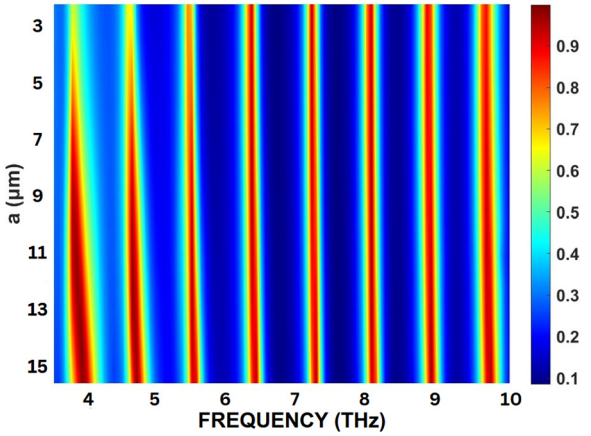

Fig. 6 Absorption spectrum *vs.* patch size '*a*' and the frequency showing maximum absorption at a = 15 μm and reduced efficiency as '*a*' decreases.

2.4. Polarization insensitivity and angular stability

The angular stability and polarization insensitivity of the proposed metasurface absorber demonstrate its robustness and efficiency in maintaining high absorption performance across varying operational conditions. Fig. 7(a) highlights the effect of changing the incidence angle θ from 0° to 50°. As θ increases, there is a slight reduction in absorption efficiency particularly at higher angles. However, the absorption remains above 95% throughout the frequency range even at θ = 50°. This high angular stability can be attributed to the careful design of the metasurface which ensures effective coupling of the incident terahertz waves with the resonant modes of the structure even at oblique incidence. Fig. 7(b) examines the effect of polarization angle ϕ that varied from 0° to 90°. The results show no noticeable change in absorption performance across the spectrum which indicates complete polarization insensitivity. This behavior arises from the symmetric geometry of the metasurface which ensures uniform interaction with incident terahertz waves irrespective of their polarization state. Polarization insensitivity is mainly governed by the isotropous response of the resonant elements like graphene patches/dielectric layers with electromagnetic waves. The consistency of the absorption characteristics across all polarization angles highlights the efficiency of the metasurface design in achieving consistent performance without the need for polarization specific tuning.

The combined effects of angular stability and polarization insensitivity make the proposed metasurface absorber a highly steadfast structure under varying operative parameters. The preservation of high absorption efficiencies at oblique

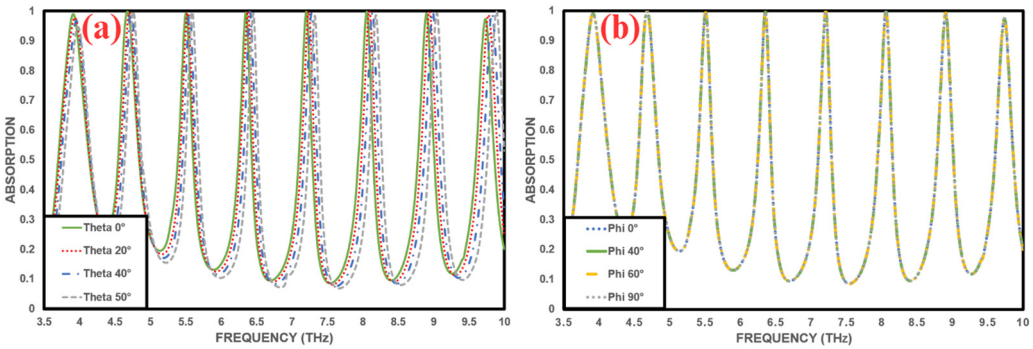

Fig. 7 (a) Absorption remains above 95% for incidence angles θ from 0° to 50°. (b) Polarization insensitivity is observed for angles ϕ from 0° to 90°.

incidence angles and across all polarization states validates the capability of the design to maintain its resonant behavior and absorption efficiency under challenging conditions. These results reflect the absorber's well-engineered structural and material properties which are augmented to provide consistent interaction with terahertz waves regardless of variations in incidence angles or polarization.

The electric field (*E*-field) distribution plays an important role in understanding the resonance mechanisms and performance of the proposed metasurface absorber. Investigating the *E*-field at various points across the spectrum provides insights into how the absorber interacts with incident electromagnetic waves to achieve high absorption efficiency. The *E*-field intensity directly links with the resonance behavior which affects the sharpness and efficiency of absorption peaks. Fig. 8 highlights the *E*-field distribution at specific resonance peaks and their corresponding dips. Fig. 8(a–d) shows the *E*-field distribution at the absorption peaks of 3.9 THz, 4.67 THz, 6.35 THz and 9.73 respectively. At these frequencies the *E*-field is highly contained and intense near the edges of the graphene patches and the surrounding dielectric material. This strong localization signifies efficient coupling between the incident terahertz waves and the resonant modes of the metamaterial which leads to maximum absorption. The sharp intensity gradients observed emphasize the high Q-factor and narrow full-width at half maximum (FWHM) achieved by the design.

Conversely, panels Fig. 8(e–h) illustrate the *E*-field distribution at the dips immediately following these peaks, at 4.4 THz, 5.15 THz, 4.7 THz and 10 THz respectively. At these dips, the *E*-field intensity is substantially reduced which indicates weaker interaction between the electromagnetic waves and the absorber structure. This reduction in *E*-field strength corresponds to the minima in the absorption spectrum that highlights the design's sharp resonance and high selectivity. The contrasting *E*-field patterns between the peaks and dips underscore the absorber's ability to effectively manipulate electromagnetic energy at targeted frequencies.

Table 1 shows a comparison of the proposed terahertz absorber with several state-of-the-art designs. The proposed absorber achieves eight distinct absorption peaks across a broad frequency range of 3.9 to 9.73 THz. With an impressive 99.3% average absorption it proposes superior efficiency compared to many existing designs. The absorber also maintains angular stability from 0° to 50°. Notably, the design provides

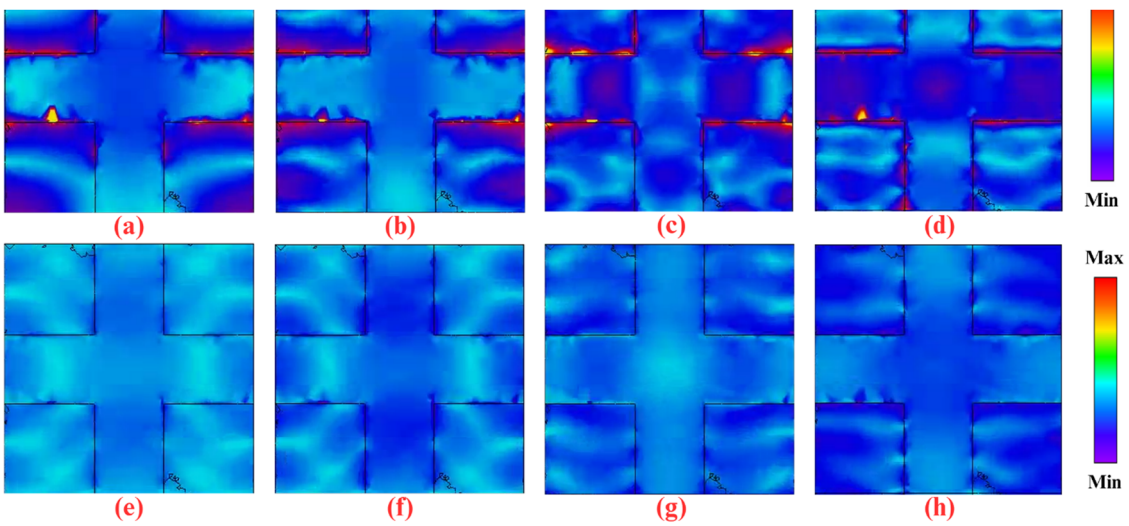

Fig. 8 Electric field distribution of the absorber. (a)–(d) show the *E*-field at resonance peaks at 04 different peaks with strong localization near the graphene patches. (e)–(h) represent the *E*-field at adjusting dips showing significantly reduced intensity.

Table 1 Comparison with different state of the art studies

Ref.	Frequency (THz)	No. of peaks	Absorption average (%)	Angular stability	Polarization insenstivity	Tunable	Year published
41	1.6, 4.42, and 4.94	3	99	0–60	Yes	No	2018
42	0.85 and 3.37	2	95.1	0–80	Yes	Yes	2018
43	7.75, 14.85, and 23.43	3	99	0–40	Yes	Yes	2019
44	0.114 and 0.181	2	98.9	0–45	Yes	No	2020
45	0.33, 0.90, 1.42, and 1.85	4	99	0–60	Yes	No	2021
46	1.36, 2.6, 3.68, and 4.36	4	98.2	0–45	Yes	No	2022
47	1.7, 2.8, 3.2, and 3.5	4	99.1	—	Yes	No	2023
48	0.865, 1.43, and 2	3	99.5	0–45	Yes	Yes	2024
49	1.99, 6, 7.37, 8.47, and 9.38	5	97.9	0–50	Yes	Yes	2024
This work	3.9, 4.67, 5.5, 6.35, 7.2, 8.05, 8.9, and 9.73	8	99.3	0–50	Yes	Yes	—

precise tuning down to very small scales and displays a total polarization insensitivity of up to 90°. These features combined with the broad frequency range and high absorption efficiency make our design a noteworthy advancement over current absorber technologies. The combination of these features *i.e.*, broad frequency coverage, exceptional absorption efficiency, angular stability, precise tunability and polarization insensitivity positions our design as a significant advancement over current terahertz absorber technologies. This innovative design addresses key challenges in the field and provides a robust solution for a wide range of applications including sensing, imaging and material characterization.

3. Conclusions

This paper introduces a highly effective and tunable terahertz absorber that reveals an innovative capability to achieve multi-band absorption with an average efficiency of 99.3% across eight distinct peaks in the 3.9 to 9.73 THz range. The integration of graphene's tunable properties heightened by the strategic inclusion of GaAs dielectric layers and a gold base reflector provides precise control over absorption frequencies through external modulation of the graphene's chemical potential. This design not only achieves exceptional absorption over a wide absorption bandwidth but also ensures polarization insensitivity and angular stability which makes it a robust and versatile solution for modern terahertz applications. The proposed absorber holds significant potential for advancing technologies in medical diagnostics, security screening, material analysis and non-destructive testing. Its innovative architecture sets a new benchmark in tunable terahertz absorbers that will lead the way for further explorations into adaptive and multifunctional metamaterials for next-generation systems.

Author contributions

The manuscript was written through contributions of both authors. Taha Sheheryar conducted the simulations and data analyses, assisted by Bo Lv, Ye Tian and Jinhui Shi. Taha Sheheryar wrote the initial manuscript, assisted and revised by Bo Lv, Ye Tian and Jinhui Shi. Both authors have read and agreed to the published version of the manuscript.

Data availability

All data supporting the findings of this study are fully provided within the article. The simulations were conducted using CST Studio Suite-2023 and all relevant results including graphs and analyses are comprehensively presented in the manuscript. No additional datasets such as those related to material characterization, fabrication or experimental testing were generated or analyzed for this study.

Conflicts of interest

There are no conflicts to declare.

Acknowledgements

B. L. was sponsored by the National Natural Science Foundation of China under Grant No. 61901133, Fundamental Research Funds for the Central Universities (3072024XX2504), and the Forward Design Technology Special Fund Project of Harbin Engineering University (KYWZ220242504 and KYWZ220240807). J. S. was sponsored by the National Natural Science Foundation of China (NSFC) (62275061, 62175049, and U22A2014), the Natural Science Foundation of Heilongjiang Province in China (ZD2020F002), the 111 Project to the Harbin Engineering University (B13015), and the Fundamental Research Funds for the Central Universities (3072022TS2509).

References

1 H.-T. Chen, *et al.*, Active terahertz metamaterial devices, *Nature*, 2006, **444**(7119), 597–600.
2 A. D'Arco, *et al.*, THz pulsed imaging in biomedical applications, *Condens. Matter*, 2020, **5**(2), 25.
3 J.-H. Son, S. J. Oh and H. Cheon, Potential clinical applications of terahertz radiation, *J. Appl. Phys.*, 2019, **125**, 19.
4 S. Yang, *et al.*, *Real-time near-field terahertz spectroscopy imaging*, *in 2021 46th International Conference on Infrared, Millimeter and Terahertz Waves (IRMMW-THz)*, 2021, IEEE.
5 J. Federici and L. Moeller, Review of terahertz and subterahertz wireless communications, *J. Appl. Phys.*, 2010, **107**, 11.
6 A. Isozaki, *et al.*, Out-of-plane actuation with a sub-micron initial gap for reconfigurable terahertz micro-electro-

mechanical systems metamaterials, *Opt. Express*, 2015, **23**(20), 26243–26251.
7 E. A. Nanni, *et al.*, Terahertz-driven linear electron acceleration, *Nat. Commun.*, 2015, **6**(1), 8486.
8 Y. Zheng, *et al.*, Numerical simulation of efficient solar absorbers and thermal emitters based on multilayer nanodisk arrays, *Appl. Therm. Eng.*, 2023, **230**, 120841.
9 W. Meng, *et al.*, Synthesis and electrochemical performance of $Li_{1+x}Ti_{2-x}Fe_x(PO_4)_3$/C anode for aqueous lithium ion battery, *Adv. Powder Technol.*, 2020, **31**(4), 1359–1364.
10 M. M. Ghods and P. Rezaei, Ultra-wideband microwave absorber based on uncharged graphene layers, *J. Electromagn. Waves Appl.*, 2018, **32**(15), 1950–1960.
11 Z. Cui, *et al.*, Dynamic tunable triple-band terahertz perfect absorber based on graphene metamaterial, *Phys. B*, 2025, **696**, 416641.
12 Q. Shangguan, *et al.*, Design of ultra-narrow band graphene refractive index sensor, *Sensors*, 2022, **22**(17), 6483.
13 C. Chen, *et al.*, PH-induced structural evolution, photodegradation mechanism and application of bismuth molybdate photocatalyst, *Adv. Powder Technol.*, 2022, **33**(12), 103858.
14 B.-X. Wang, *et al.*, Design of a four-band and polarization-insensitive terahertz metamaterial absorber, *IEEE Photonics J.*, 2014, **7**(1), 1–8.
15 A. Beheshti Asl, D. Pourkhalil, A. Rostami and H. Mirtaghioglu, A perfect electrically tunable graphene-based metamaterial absorber, *J. Comput. Electron.*, 2021, **20**, 864–872.
16 C. Huang, *et al.*, Simultaneous control of absorbing frequency and amplitude using graphene capacitor and active frequency-selective surface, *IEEE Trans. Antennas Propag.*, 2020, **69**(3), 1793–1798.
17 Z. Ding, *et al.*, Design of an ultra-broadband terahertz absorber based on a patterned graphene metasurface with machine learning, *J. Mater. Chem. C*, 2023, **11**(17), 5625–5633.
18 J. Song, *et al.*, Broadband and tunable radar absorber based on graphene capacitor integrated with resistive frequency-selective surface, *IEEE Trans. Antennas Propag.*, 2019, **68**(3), 2446–2450.
19 Z. Zhai, L. Zhang, X. Li and S. Xiao, Tunable terahertz broadband absorber based on a composite structure of graphene multilayer and silicon strip array, *Opt. Commun.*, 2019, **431**, 199–202.
20 Y. M. Qing, H. F. Ma and T. J. Cui, Tailoring anisotropic perfect absorption in monolayer black phosphorus by critical coupling at terahertz frequencies, *Opt. Express*, 2018, **26**(25), 32442–32450.
21 R. Zheng, *et al.*, Ultra wideband tunable terahertz metamaterial absorber based on single-layer graphene strip, *Diamond Relat. Mater.*, 2024, **141**, 110713.
22 Q. Wang, *et al.*, Switchable quadruple narrowband to broadband terahertz perfect absorber based on graphene and VO2 metamaterials, *Diamond Relat. Mater.*, 2024, **142**, 110832.
23 S. Cao, *et al.*, Graphene–silver hybrid metamaterial for tunable and high absorption at mid-infrared waveband, *IEEE Photonics Technol. Lett.*, 2018, **30**(5), 475–478.
24 S. K. Patel, *et al.*, Graphene-based highly efficient and broadband solar absorber, *Opt. Mater.*, 2019, **96**, 109330.
25 B. Xu, *et al.*, A novel absorber with tunable bandwidth based on graphene, *IEEE Antennas Wirel. Propag. Lett.*, 2014, **13**, 822–825.
26 H. Tian, *et al.*, Interface-induced high responsivity in hybrid graphene/GaAs photodetector, *Adv. Opt. Mater.*, 2020, **8**(8), 1901741.
27 Z. Chen, *et al.*, Improved optical damage threshold graphene Oxide/SiO_2 absorber fabricated by sol-gel technique for mode-locked erbium-doped fiber lasers, *Carbon*, 2019, **144**, 737–744.
28 R. Zhou, *et al.*, Tunable broadband terahertz absorber based on graphene metamaterials and VO_2, *Opt. Mater.*, 2021, **114**, 110915.
29 S. K. Patel, *et al.*, Graphene-based plasmonic absorber for biosensing applications using gold split ring resonator metasurfaces, *J. Light Technol.*, 2021, **39**(17), 5617–5624.
30 M. R. Nickpay, M. Danaie and A. Shahzadi, A wideband and polarization-insensitive graphene-based metamaterial absorber, *Superlattices Microstruct.*, 2021, **150**, 106786.
31 Y. Zhang, *et al.*, Graphene induced tunable and polarization-insensitive broadband metamaterial absorber, *Opt. Commun.*, 2017, **382**, 281–287.
32 X. Chen, *et al.*, Graphene hybrid structures for integrated and flexible optoelectronics, *Adv. Mater.*, 2020, **32**(27), 1902039.
33 H. Zhang, M. Chhowalla and Z. Liu, 2D nanomaterials: graphene and transition metal dichalcogenides, *Chem. Soc. Rev.*, 2018, **47**(9), 3015–3017.
34 P. Zamzam and P. Rezaei, A terahertz dual-band metamaterial perfect absorber based on metal-dielectric-metal multi-layer columns, *Opt. Quantum Electron.*, 2021, **53**, 1–9.
35 B. Khodadadi, P. Rezaei, V. Ghods and M. Babaeinik, Wideband polarization-insensitive metamaterial perfect absorber based on bilayer graphene metasurface, *Opt. Quantum Electron.*, 2022, **54**(11), 739.
36 H. Lv, *et al.*, A brief introduction to the fabrication and synthesis of graphene based composites for the realization of electromagnetic absorbing materials, *J. Mater. Chem. C*, 2017, **5**(3), 491–512.
37 J. Zhang, *et al.*, Towards photodetection with high efficiency and tunable spectral selectivity: graphene plasmonics for light trapping and absorption engineering, *Nanoscale*, 2015, **7**(32), 13530–13536.
38 F. Qin, *et al.*, Design of high efficiency perovskite solar cells based on inorganic and organic undoped double hole layer, *Sol. Energy*, 2023, **262**, 111796.
39 K.-T. Lin, H. Lin, T. Yang and B. Jia, Structured graphene metamaterial selective absorbers for high efficiency and omnidirectional solar thermal energy conversion, *Nat. Commun.*, 2020, **11**(1), 1389.
40 Y. Cheng, *et al.*, Terahertz narrowband perfect metasurface absorber based on micro-ring-shaped GaAs array for enhanced refractive index sensing, *Phys. E*, 2023, **146**, 115527.
41 X. Huang, *et al.*, Multiband ultrathin polarization-insensitive terahertz perfect absorbers with complementary metamaterial and resonator based on high-order electric and magnetic resonances, *IEEE Photonics J.*, 2018, **10**(6), 1–11.

42 M. Huang, *et al.*, Based on graphene tunable dual-band terahertz metamaterial absorber with wide-angle, *Opt. Commun.*, 2018, **415**, 194–201.
43 Z. Yi, *et al.*, Graphene-based tunable triple-band plasmonic perfect metamaterial absorber with good angle-polarization-tolerance, *Results Phys.*, 2019, **13**, 102149.
44 W. Li and Y. Cheng, Dual-band tunable terahertz perfect metamaterial absorber based on strontium titanate (STO) resonator structure, *Opt. Commun.*, 2020, **462**, 125265.
45 A. Veeraselvam, G. N. A. Mohammed, K. Savarimuthu and R. Sankararajan, A novel multi-band biomedical sensor for THz regime., *Opt. Quantum Electron.*, 2021, **53**, 1–20.
46 S. A. Khatami, P. Rezaei and P. Zamzam, Quad band metal-dielectric-metal perfect absorber to selective sensing application, *Opt. Quantum Electron.*, 2022, **54**(10), 638.
47 R. Bhati and A. K. Malik, Multiband terahertz metamaterial perfect absorber for microorganisms detection, *Sci. Rep.*, 2023, **13**(1), 19685.
48 S. Hadipour and P. Rezaei, Retracted article: A graphene-based triple-band THz metamaterial absorber for cancer early detection, *Opt. Quantum Electron.*, 2023, **55**(13), 1122.
49 R. Lai, *et al.*, Design of a Penta-Band Graphene-Based Terahertz Metamaterial Absorber with Fine Sensing Performance, *Micromachines*, 2023, **14**(9), 1802.

